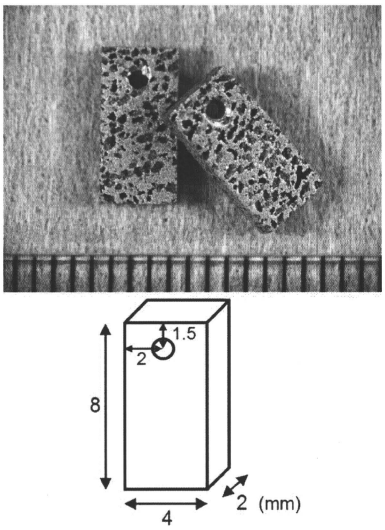

Figure 1. Photograph and design drawing of porous titanium implants used in this study. [Color figure can be viewed in the online issue, which is available at www.interscience.wiley.com.]

MATERIALS AND METHODS

Preparation of porous titanium

Sintered porous titanium implants (porosity 50%; average pore size ± standard deviation 303 ± 152 μm) were supplied by Osaka Yakin Co., Ltd (Japan) and were manufactured through sintering of titanium powders added with volatile spacer particles (ammonium hydrogen carbonate) as previously described.[14–17] For animal experiments, rectangular plate-shaped implants (4 mm × 8 mm × 2 mm) were cut from the sintered body using electric-discharge machining, and a hole (1 mm in diameter) was made on each implant (Fig. 1).

Bioactive surface treatment and loading of BMP-2

For bioactive treatments, the titanium substrates were immersed in aqueous 5*M* NaOH solution at 60°C for 24 h, 0.5 m*M* HCl at 40°C for 24 h, ultrapure water at 40°C for 24 h, and then heat-treated at 600°C for 1 h, as previously described.[14,17] The homogeneity of the bioactive surface was confirmed by examining the topography and composition of the center and peripheral parts of several implants using a scanning electron microscope (SEM), an energy dispersive X-ray microanalyzer connected to the SEM, and X-ray diffractometry. *In vitro* apatite-forming ability was confirmed by soaking samples in simulated body fluid[18] for 3 d.

After sterilization in ethylene oxide, half of the implants were soak-loaded with 5 μg of recombinant human BMP-2 (Astellas Pharma Inc., Japan) and were freeze-dried before surgery.

Animal experiments

Sixteen Japanese white male rabbits weighing between 2.7 and 3.0 kg underwent operations. Intravenous injection of pentobarbital sodium (70 mg/kg) and local administration of 0.5% lidocaine (20 mg) was used for anesthesia. Animals were placed in a supine position, and the bilateral patellar tendon was exposed in an aseptic manner. A slit was made in the coronal plane to divide it into anterior and posterior halves, and an implant was inserted into the tendon slit with its hole located proximally [Fig. 2(a)]. Eight animals received 16 implants without BMP-2 (B− group), and eight animals received 16 implants loaded with BMP-2 (B+ group). After implantation, the bilateral edge of each tendon was sutured to prevent implant migration and also to seal the implant within the tendon tissue. The animals were kept individually in cages without immobilization until euthanasia.

Four animals in each group were euthanized with intravenous pentobarbital sodium at 4 weeks postoperation, and the remaining animals were euthanized after 8 weeks. Thus, eight samples from each group were harvested for each implantation period. Six were used for quantitative evaluation using mechanical tests and histomorphometric analyses. The remaining two samples were used to represent the typical histology of each group. This animal study

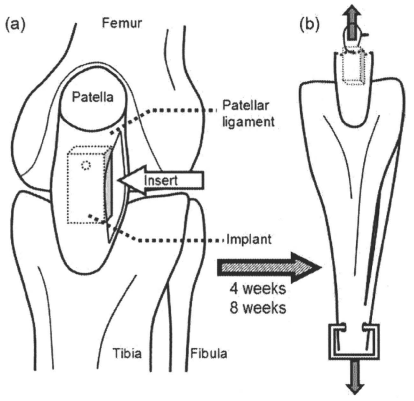

Figure 2. Schematic diagram of experimental methods. (a) A porous titanium implant was inserted into the slit of tendon. (b) Mechanical tests were performed to evaluate the pull-out failure load at 4 and 8 weeks after surgery.

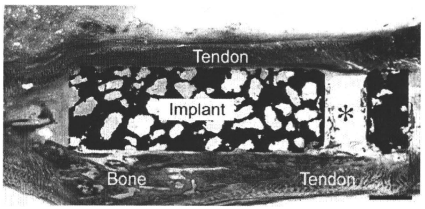

Figure 3. Calculation of bone coverage rate. Bone coverage rate (%) = (length of yellow dot line)/(length of white dot line) × 100. * The hole that wire was passed through for the mechanical test. The bone coverage rate was measured on the area distal to the hole. Scale = 1 mm. [Color figure can be viewed in the online issue, which is available at www.interscience.wiley.com.]

was approved by the Animal Research Committee, Graduate School of Medicine, Kyoto University, Japan.

Mechanical tests

Patellar tendons, including the implant, and tibial bone were harvested *en bloc* for evaluation of the attachment strength between the implant and the tendon. The implant surface proximal to the hole was exposed, and a 24G soft wire ~20 cm in length was inserted into the hole and was looped. The pull-out failure load of the tendon/implant complex was measured by pulling the soft wire and a hook attached to the distal end of tibia at a cross-head speed of 35 mm/min [Fig. 2(b)]. The failure load (N) was recorded using an Instron-type autograph (Model 1011, Aikoh Engineering Co., Ltd, Japan), and the results are presented as mean ± standard deviation.

Histomorphometric and histological analyses

After the mechanical tests, the implants were reduced into the tendons, and the tendons were resected from the tibiae at the insertion. Specimens were fixed in 10% phosphate-buffered formalin, dehydrated in ethanol at serial concentrations, and embedded in polyester resin. Sections 500 μm in thickness were cut with a band saw (Microcutting machine BS-3000S, EXACT, Germany) in the sagittal plane. The middle sections were ground to a 40 μm thickness using a grinding-sliding machine (Microgrinding machine MG-4000, EXACT, Germany) and stained with Stevenel's blue and Van Gieson's picrofuchsin. They were observed by light microscopy (Eclipse 80i, Nikon, Japan) and fluorescence microscopy (IX70, Olympus, Japan), and were recorded with digital cameras. Histomorphometric analyses were performed on the area distal to the hole using Adobe Photoshop 6.0 (Adobe Systems Inc., USA) and ImageJ (National Institutes of Health, USA). The bone area around and within the implant (mm^2) was separately measured using fluorescence microphotographs.[16] Bone coverage rate (%) was defined as the percentage of length of implant surface covered with bone or cartilage to length of total implant surface (Fig. 3). Using Statcel software,[19] the results were analyzed statistically by an unpaired t-test. Differences with a $p < 0.05$ were considered statistically significant.

For histological observation, implants were harvested with surrounding tendon tissue after euthanasia and were not subjected to mechanical testing. After being embedded in polyester resin, they were sectioned, ground, stained, and recorded in the same way.

RESULTS

Mechanical tests

Results of the mechanical tests are summarized in Figure 4. The pull-out failure load of the B− and B+ groups were 9.3 ± 2.7 N and 25.1 ± 8.4 N at 4 weeks ($n = 6$, $p < 0.005$); and 12.9 ± 3.2 N and 142.4 ± 33.9 N at 8 weeks ($n = 6$, $p < 0.0001$), respectively. Macroscopically, implant failure did not occur during the mechanical test. Failure occurred mostly at the interface between the implant and the surrounding tissue or within the bone. Tendinous tissue was rarely found to remain on the outer surface of the implants.

Histological and histomorphometric analyses

In the B− group, no new bone was histologically found at the interface between the tendon and the implant, and the two elements appeared to be attached directly to each other [Fig. 5(a)]. A tiny bone was found within a pore in one B− sample after 8 weeks [Fig. 5(b)]. On the other hand, new bone was abundantly found in the B+ group. After 4 weeks, bone formed mainly around the implants and rarely within the pores [Fig. 6(a)]. After 8 weeks,

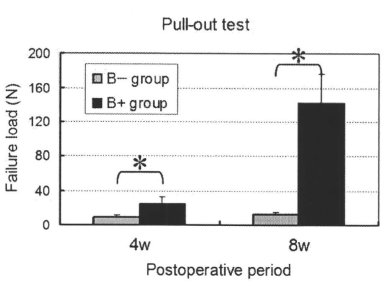

Figure 4. Results of the mechanical test. Differences between values of the B− group and the B+ group were significant at both postoperative periods (*$p < 0.05$).

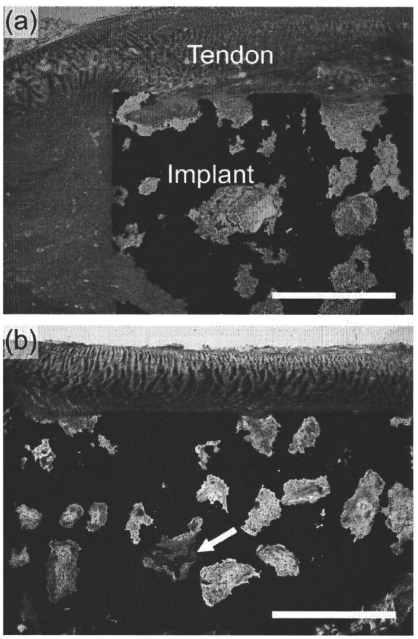

Figure 5. Histology of the B− group. (a) Sample without mechanical test; (b) after mechanical test. No new bone was found around the implants (a). A tiny new bone was found within a pore in one sample after 8 weeks (b, arrow). Scale = 1 mm. [Color figure can be viewed in the online issue, which is available at www.interscience. wiley. com.]

new bone was found also within the pores and was in contact with the inner surface of the implant [Fig. 6(b)]. Although direct attachment between the bone and the outer surface of the implant was rare after only 4 weeks, it was common after 8 weeks. At 8 weeks, new bone contained marrow-like tissue and appeared more mature than at 4 weeks.

At the tendon–bone interface, fibrocartilage cells were found in some places [Fig. 7(a)]. They were embedded in both mineralized and unmineralized matrices, and were arranged in rows parallel to the direction of the tendon fibers. Dense collagen fibers were also found at the tendon–bone interface [Fig. 7(b)]. They were arranged perpendicular to the interface and parallel to the direction of the tendon fibers.

Bone area around the implant in the B− group and the B+ group was 0 ± 0 and 2.6 ± 1.6 mm^2 at 4 weeks (n = 6) and 0 ± 0 and 6.0 ± 3.1 mm^2 at 8 weeks [n = 6, Fig. 8(a)], respectively. Bone area within the implant pores was 0 ± 0 and 0.039 ± 0.058 mm^2 at 4 weeks (n = 6) and 0.0075 ± 0.018 and 1.1 ± 0.45 mm^2 at 8 weeks [n = 6, Fig. 8(a)], respectively. Bone coverage rates of the two groups were 0 ± 0 and 54.9 ± 18.2% at 4 weeks (n = 6) and 0 ± 0 and 73.5 ± 18.4% at 8 weeks [n = 6, Fig. 8(b)], respectively.

DISCUSSION

A simple experimental model was established in this study to evaluate the attachment between the tendon and the metal histologically and mechani-

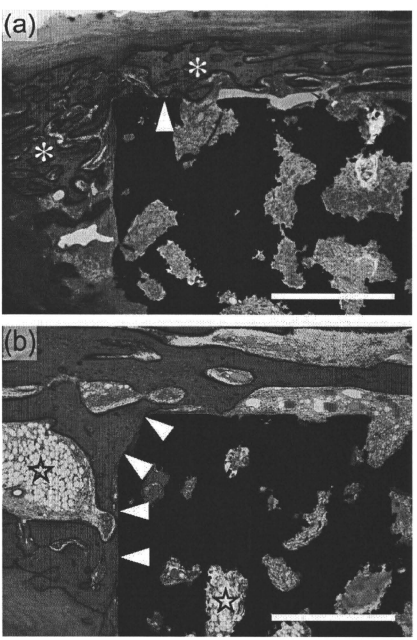

Figure 6. Histology of the B+ group. New bone was formed around the implants (asterisk), but was rarely found within pores after only 4 weeks (a). Increasing amounts of new bone were found both around and within implants after 8 weeks (b). Newly formed bone appeared to be more mature with marrow-like tissue (star), and have a greater area of direct attachment with the outer surface of implants (arrow head) at 8 weeks than at 4 weeks. Scale = 1 mm. [Color figure can be viewed in the online issue, which is available at www.interscience.wiley.com.]

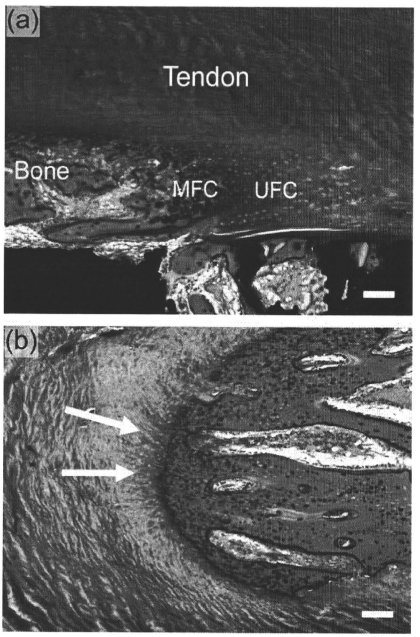

Figure 7. Histology of bone–tendon interface. Mineralized fibrocartilage (MFC) and unmineralized fibrocartilage (UFC) lie between bone and tendon (a). Dense collagen fibers (arrow) were found at the interface between bone and tendon (b). Scale = 100 μm. [Color figure can be viewed in the online issue, which is available at www.interscience.wiley.com.]

cally. Although the initial fixation and the implanting method of the current model did not imitate clinical conditions, the results were reproducible and reliable. Our findings clearly show that bioactive porous titanium can attach directly and firmly to tendon via ectopically formed bone when BMP-2 is supplemented. In comparison with experimental models in previous studies of tendon attachment to metal,[5–9] our model was more feasible in that implant preparation and operative methods were simple and easy, the experimental period was short, and animal welfare was of high priority.

Histologically, no new bone was found within or around implants of the B− group except in one sample, and the implants were totally surrounded by tendon or scar tissue (Fig. 5). According to previous reports, it took at least 3 months to confirm ectopic bone formation within the pores of the bioactive porous titanium in the back muscle of beagle dogs,[14] and ectopic bone formation could rarely be observed in rodents.[20,21] It is reasonable that almost no new bone was found after only 8 weeks in this study. Although the tendon was histologically in direct contact with the outer surface of the implant, their interface was revealed to be weak by mechanical testing.

On the other hand, new bone was significantly formed in the B+ group not only within pores of implants, but also around them (Figs. 5, 6, 8a), and the pull-out strength of the tendon/implant complex was successfully reinforced. Interestingly, new bone formation was more vigorous around the implant than within the pores (Figs. 6, 8a). These findings support that the *in vivo* environment around the implant was more preferable for new bone formation than that within the pores. It is our speculation that precursor cells and matrices available for new bone formation were more abundant around the implant. The most meaningful finding in this study is that simple loading of BMP-2 can result in reinforcing tendon attachment to bioactive porous titanium.

It is remarkable that ectopic bone was efficiently formed, although no degradable carrier for the con-

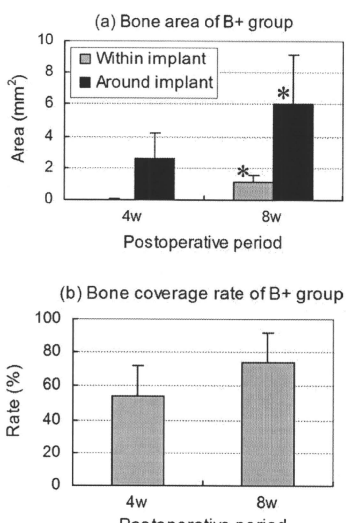

Figure 8. Results of histomorphometry of B+ group. (a) New bone area within and around the implant significantly increased during the observation period (*$P < 0.05$). (b) Bone coverage rate also increased during the observation period. The rate at 4 and at 8 weeks was different ($P = 0.095$).

trolled release of BMP-2 was used in this study. In our preliminary study, it was found that BMP-2 was poorly released from the implant *in vitro*. The bioactive-treated surface may have a high affinity for BMP-2. In general, a local and controlled delivery system is necessary for ectopic bone formation by BMP-2.[22] Collagen impregnation and hydroxyapatite coating are popular methods for controlled release of agents from metallic materials.[23] However, they have disadvantages such as disease transmission, alteration to macropore topography, and delamination *in vivo*.[24] We demonstrate that bioactive porous titanium does not require such additional treatment for new bone formation by BMP-2.

Histologically, fibrocartilage and dense collagen fibers were found at the tendon–bone interface in the B+ group (Fig. 7). Because failure at this interface was not found by the pull-out test, we speculate that this interface's strength may result from regeneration of biological enthesis-like structures.[7,25] The overall strength of the tendon/implant complex depended on the strength of the bone–implant interface and of the bone itself, corresponding to mechanical test failure in that area. The area of direct attachment between the bone and the implant increased as the bone matured (Fig. 6). As well as bone volume and coverage rate, the maturity of the bone was considered to influence the bone–implant interface.

Yamamoto et al. reported that 34 μg of BMP-2/cm^3 of hydrogel was sufficient to enhance bone regeneration.[26] According to their study, the required dose of BMP-2 in our model was only 2.176 μg/implant. However, we found that 3 μg of BMP-2/implant was insufficient for new bone formation in our preliminary study, and decided to use 5 μg/implant in this study.

The experimental model used in this study has some limitations, for instance that the initial fixation does not imitate clinical conditions. However, it would be beneficial to conduct further research into the method of forming firm attachments quickly using this simple and easy model. For example, grafting bone chips or artificial bone granules around the BMP-2-loaded implant could improve the results, because it would provide substrates and void spaces for bone formation. A combination of BMPs and allogenic bone graft has already been shown to have synergic effects on bone formation.[9,27] In addition, modification of the bioactive treatment would influence the attachment strength by several mechanisms. It would vary the bioactivity of the implant surface, the attachment strength per unit area,[10] and the drug release profile. Additional studies using the current model will discover better materials and methods to form a firm attachment rapidly before moving into clinical studies.

CONCLUSIONS

An experimental model was established in this study to evaluate the attachment between the tendon and the metal. Our findings show that attachment between the bioactive porous titanium and the tendon can be significantly reinforced by BMP-2-induced ectopic bone formation. We expect that a simple combination of bioactive porous titanium and BMP-2 will contribute to a better joint function when used in the metal prosthesis.

References

1. Damron TA. Endoprosthetic replacement following limb-sparing resection for bone sarcoma. Semin Surg Oncol 1997;13:3–10.
2. Frankle MA, Mighell MA. Techniques and principles of tuberosity fixation for proximal humeral fractures treated with hemiarthroplasty. J Shoulder Elbow Surg 2004;13:239–247.
3. Ahmed IM, Lagopoulos M, Mcconnell P, Soames RW, Sefton GK. Blood supply of the Achilles tendon. J Orthop Res 1998;16:591–596.
4. Fenwick SA, Hazleman BL, Riley GP. The vasculature and its role in the damaged and healing tendon. Arthritis Res 2002;4:252–260.
5. Reach JS, Dickey ID, Zobitz ME, Adams JE, Scully SP, Lewallen DG. Direct tendon attachment and healing to porous tantalum: An experimental animal study. J Bone Joint Surg Am 2007;89:1000–1009.
6. Gottsauner-Wolf F, Egger EL, Giurea A, Antosch M, Olsen D, Rock MG, Sim FH. Biologic attachment of an allograft bone and tendon transplant to a titanium prosthesis. Clin Orthop Relat Res 1999;101–110.
7. Inoue N, Ikeda K, Aro HT, Frassica FJ, Sim FH, Chao EY. Biologic tendon fixation to metallic implant augmented with autogenous cancellous bone graft and bone marrow in a canine model. J Orthop Res 2002;20:957–966.
8. Oddy MJ, Pendegrass CJ, Goodship AE, Cannon SR, Briggs TW, Blunn GW. Extensor mechanism reconstruction after proximal tibial replacement. J Bone Joint Surg Br 2005;87:873–878.
9. Higuera CA, Inoue N, Lim JS, Zhang R, Dimaano N, Frassica FJ, Chao EY. Tendon reattachment to a metallic implant using an allogenic bone plate augmented with rhOP-1 vs. autogenous cancellous bone and marrow in a canine model. J Orthop Res 2005;23:1091–1099.
10. Fujibayashi S, Nakamura T, Nishiguchi S, Tamura J, Uchida M, Kim HM, Kokubo T. Bioactive titanium: Effect of sodium removal on the bone-bonding ability of bioactive titanium prepared by alkali and heat treatment. J Biomed Mater Res 2001;56:562–570.
11. Nishiguchi S, Kato H, Fujita H, Oka M, Kim HM, Kokubo T, Nakamura T. Titanium metals form direct bonding to bone after alkali and heat treatments. Biomaterials 2001;22:2525–2533.
12. Fujibayashi S, Neo M, Kim HM, Kokubo T, Nakamura T. Osteoinduction of porous bioactive titanium metal. Biomaterials 2004;25:443–450.
13. Takemoto M, Fujibayashi S, Neo M, Suzuki J, Kokubo T, Nakamura T. Mechanical properties and osteoconductivity of porous bioactive titanium. Biomaterials 2005;26:6014–6023.
14. Takemoto M, Fujibayashi S, Neo M, Suzuki J, Matsushita T, Kokubo T, Nakamura T. Osteoinductive porous titanium

implants: Effect of sodium removal by dilute HCl treatment. Biomaterials 2006;27:2682–2691.
15. Wen CE, Mabuchi M, Yamada Y, Shimojima K, Chino Y, Asahina T. Processing of biocompatible porous Ti and Mg. Scr Mater 2001;45:1147–1153.
16. Otsuki B, Takemoto M, Fujibayashi S, Neo M, Kokubo T, Nakamura T. Pore throat size and connectivity determine bone and tissue ingrowth into porous implants: Three-dimensional micro-CT based structural analyses of porous bioactive titanium implants. Biomaterials 2006;27:5892–5900.
17. Takemoto M, Fujibayashi S, Neo M, So K, Akiyama N, Matsushita T, Kokubo T, Nakamura T. A porous bioactive titanium implant for spinal interbody fusion: an experimental study using a canine model. J Neurosurg Spine 2007;7:435–443.
18. Kokubo T, Kushitani H, Sakka S, Kitsugi T, Yamamuro T. Solutions able to reproduce in vivo surface-structure changes in bioactive glass-ceramic A-W. J Biomed Mater Res 1990;24:721–734.
19. Yanai H. 4 Steps, Excel Statistics, Tokyo: OMS; 1998.
20. Kurashina K, Kurita H, Wu Q, Ohtsuka A, Kobayashi H. Ectopic osteogenesis with biphasic ceramics of hydroxyapatite and tricalcium phosphate in rabbits. Biomaterials 2002;23:407–412.
21. Yuan H, Van Blitterswijk CA, De Groot K, De Bruijn JD. Cross-species comparison of ectopic bone formation in biphasic calcium phosphate (BCP) and hydroxyapatite (HA) scaffolds. Tissue Eng 2006;12:1607–1615.
22. Seeherman H, Wozney JM. Delivery of bone morphogenetic proteins for orthopedic tissue regeneration. Cytokine Growth Factor Rev 2005;16:329–345.
23. Liu Y, De Groot K, Hunziker EB. Osteoinductive implants: The mise-en-scene for drug-bearing biomimetic coatings. Ann Biomed Eng 2004;32:398–406.
24. Lappalainen R, Santavirta SS. Potential of coatings in total hip replacement. Clin Orthop Relat Res 2005;430:72–79.
25. Pendegrass CJ, Oddy MJ, Cannon SR, Briggs T, Goodship AE, Blunn GW. A histomorphological study of tendon reconstruction to a hydroxyapatite-coated implant: Regeneration of a neo-enthesis in vivo. J Orthop Res 2004;22:1316–1324.
26. Yamamoto M, Takahashi Y, Tabata Y. Enhanced bone regeneration at a segmental bone defect by controlled release of bone morphogenetic protein-2 from a biodegradable hydrogel. Tissue Eng 2006;12:1305–1311.
27. Hidaka C, Goshi K, Rawlins B, Boachie-Adjei O, Crystal RG. Enhancement of spine fusion using combined gene therapy and tissue engineering BMP-7-expressing bone marrow cells and allograft bone. Spine 2003;28:2049–2057.

Author's personal copy

J Mater Sci: Mater Med (2011) 22:273–278
DOI 10.1007/s10856-010-4218-y

Effect of heat treatments on apatite-forming ability of NaOH- and HCl-treated titanium metal

Deepak K. Pattanayak · Seiji Yamaguchi · Tomiharu Matsushita · Tadashi Kokubo

Received: 6 October 2010 / Accepted: 11 December 2010 / Published online: 29 December 2010
© Springer Science+Business Media, LLC 2010

Abstract Titanium (Ti) metal was soaked in HCl solution after NaOH treatment and then subjected to heat treatments at different temperatures. Their apatite-forming abilities in a simulated body fluid (SBF) were discussed in terms of their surface structures and properties. The nanometer scale roughness formed on Ti metal after NaOH treatment remained after the HCl treatment and a subsequent heat treatment below 700°C. Hydrogen titanate was formed on Ti metal from an HCl treatment after NaOH treatment, and this was converted into titanium oxide of anatase and rutile phases by a subsequent heat treatment above 500°C. The scratch resistance of the surface layer increased with the formation of the titanium oxide after a heat treatment up to 700°C, and then decreased with increasing temperature. The Ti metal with a titanium oxide layer formed on its surface showed a high apatite-forming ability in SBF when the heat treatment temperature was in the range 500–700°C. The high apatite-forming ability was attributed to the positive surface charge in an SBF. These positive surface charges were ascribed to the presence of chloride ions, which were adsorbed on the surfaces and dissociated in the SBF to give an acid environment.

1 Introduction

Titanium (Ti) metal and its alloys are widely used as various implants in orthopedic and dental fields because of their high mechanical strength and good biocompatibility [1]. However, they do not bond to living bone [2]. Early on, it was shown that Ti metal forms a bone-like apatite layer on its surface in the living body, and bonds to living bone through this apatite layer, if it is subjected to NaOH and heat treatment to form sodium titanate on its surface [3–6]. These treatments have been applied to the porous layer of an artificial hip joint and the resulting implant has been used clinically in Japan since 2007 [7].

Later it was also found that Ti metal forms the bone-like apatite on its surface in a simulated body fluid (SBF), even if it is soaked in water or HCl solution after the NaOH treatment and then heat-treated at 600°C to form titanium oxide on its surface [8]. Its apatite-forming ability increased with increasing concentration of the HCl solution, and assumed to be attributed to positive surface charge of the Ti metal increased with increasing concentration of the HCl solution [8].

In this study, Ti metal was soaked in 50 mM HCl solution after the NaOH treatment and then subjected to heat treatment at different temperatures. Their apatite-forming abilities in SBF were discussed in terms of their surface structures and properties. Much attention has been paid on bioactive Ti metal prepared by HCl and heat treatments after the NaOH treatment, because a porous Ti metal subjected to these treatments was found to exhibit osteoconductivity [9] as well as osteoinductivity [10]. It is already being subjected to clinical trial for application to spinal fusion devices [11].

2 Materials and methods

2.1 Preparation of specimens

Commercially pure Ti metal (Kobe Steel, Ltd., Japan) was cut into rectangular samples (dimensions = 10 × 10 × 1 mm^3),

D. K. Pattanayak (✉) · S. Yamaguchi · T. Matsushita · T. Kokubo
Department of Biomedical Sciences, College of Life and Health Sciences, Chubu University, 1200 Matsumoto-cho, Kasugai 487-8501, Japan
e-mail: deepak@isc.chubu.ac.jp; deepak_pattanayak@rediffmail.com

Author's personal copy

abraded with a #400 diamond plate, washed with acetone, 2-propanol, and ultrapure water for 30 min each in an ultrasonic cleaner, and then dried overnight in an oven at 40°C. The samples were then soaked in 5 ml of a 5 M NaOH solution at 60°C in an oil bath while being shaken at 120 strokes/min for a period of 24 h, and then gently washed with ultrapure water. Subsequently, the samples were soaked in 10 ml of a 50 mM HCl solution at 40°C in an oil bath while being shaken at 120 strokes/min for a period of 24 h. The samples were then gently washed with ultrapure water and dried overnight in an oven at 40°C. The samples were heated to several temperatures in the range 400–800°C at a rate of 5°C/min in Fe–Cr electric furnace in air, maintained at the desired temperature for a period of 1 h, and then allowed to cool at the natural rate of the furnace to room temperature. For the present study, ten samples were prepared in each heat treatment condition.

2.2 Examination of the apatite-forming ability in an SBF

The samples subjected to NaOH, HCl, and heat treatments were soaked at 36.5°C in 30 ml of an acellular SBF with ion concentrations nearly equal to those of human blood plasma (Na^+ 142.0, K^+ 5.0, Mg^{2+} 1.5, Ca^{2+} 2.5, Cl^- 147.8, HCO_3^- 4.2, HPO_4^{2-} 1.0, and SO_4^{2-} 0.5 mM). The SBF was prepared by dissolving reagent grade NaCl, $NaHCO_3$, KCl, $K_2HPO_4{\cdot}3H_2O$, $MgCl_2{\cdot}6H_2O$, $CaCl_2$, and Na_2SO_4 (Nacalai Tesque, Inc., Japan) in ultrapure water, and the solution was buffered at pH = 7.40 using tris (hydroxymethyl) aminomethane [$(CH_2OH)_3CNH_2$] and 1 M HCl (Nacalai Tesque, Inc.) [12]. The samples were removed from the SBF after 1 day, gently washed with ultrapure water, and dried in an oven at 40°C. The formation of apatite on the surface of the samples was examined using scanning electron microscopy (SEM) and thin film X-ray diffraction (TF-XRD) using the methods described in the next section.

2.3 Surface analysis of treated Ti metals

The surface of the Ti metals subjected to NaOH, HCl, and heat treatments, and those subsequently soaked in an SBF for several periods were analyzed using TF-XRD (TF-XRD; RINT-2500, Rigaku Co., Japan) and X-ray photoelectron spectroscopy (XPS; ESCA-3300KM, Shimadzu Co., Japan). In the TF-XRD experiments, CuKα radiation was used as the X-ray source, and the angle of the incident beam was 1° against the sample surface. In the XPS experiments, MgKα radiation was used as the X-ray source (λ = 9.8903 Å). The XPS takeoff angle was set at 45°, which enabled the system to detect photoelectrons to a depth of 5–10 nm from the surface of the substrate. The binding energy of the measured spectra was calibrated by reference to the C_{1s} peak of the surfactant's CH_2 group on the substrate occurring at 284.6 eV.

The sample surfaces were coated with a Pt/Pd film and observed under a field emission scanning electron microscope (FE-SEM; Hitachi S-4300, Hitachi Co., Japan) using an acceleration voltage of 15 kV.

The scratch resistance of the surfaces of the treated Ti metals was measured using a scratch tester (CSR-2000; Rhesca Co., Ltd., Japan). In this measurement, a stylus with diamond tip was moved on the sample surface at a speed of 10 mm/s under an applied load of 100 mN/min. The critical scratch load was estimated from an abrupt change in the signal of the sensor output, which indicated a complete peeling of the surface layer.

The zeta potential of the treated Ti metals was measured using plate samples (dimensions = 13 × 33 × 1 mm^3). In the preparation of these plate samples, 20 ml of the NaOH solution and 30 ml of the HCl solution were used. The Ti metal samples were first grounded to allow for leakage of any stray charge, and were then immediately set in a zeta potential and particle size analyzer (ELS-Z1, Otsuka Electronics Co., Japan) using a glass cell for the plate sample. The zeta potential was measured under an applied voltage of 40 V in a 10 mM NaCl solution with dispersed monitor particles composed of polystyrene latex particles (diameter = 500 nm) coated with hydroxyl propyl cellulose. Five samples were measured for each experimental condition, and the average values were used in the analysis.

3 Results

3.1 Surface structure of the treated Ti metal

Figure 1 shows FE-SEM photographs of the surface of Ti metal subjected to heat treatments at various temperatures after NaOH and HCl treatments. A fine network structure on the nanometer scale formed on the surface of the Ti metal after the initial NaOH treatment, and this remained essentially unchanged after the subsequent HCl and heat treatments up to 700°C, but began to fade for a heat treatment of 800°C.

Figure 2 shows the TF-XRD patterns of surface of Ti metal subjected to heat treatment at various temperatures after NaOH and HCl treatments. From Fig. 2, it can be seen that hydrogen titanate ($H_2Ti_3O_7$) had formed on the Ti metal surface after the NaOH and HCl treatments [8, 13, 14], and that this phase had converted to anatase and rutile after subsequent heat treatments above 500°C. The ratio of rutile to anatase increased with increasing heat treatment temperature, and only rutile was detected for a heat treatment temperature of 800°C.

Figure 3 shows the scratch resistance of the surface of Ti metal subjected to heat treatments at various

Author's personal copy

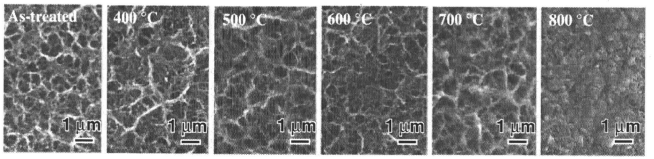

Fig. 1 FE-SEM photographs of surface of Ti metals subjected to heat treatments after NaOH and HCl treatments at various temperatures

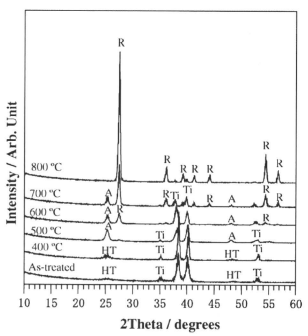

Fig. 2 TF-XRD patterns of surfaces of Ti metals subjected to heat treatments at various temperatures after NaOH and HCl treatments. *Ti* α Titanium, *HT* Hydrogen titanate, *A* anatase, *R* Rutile

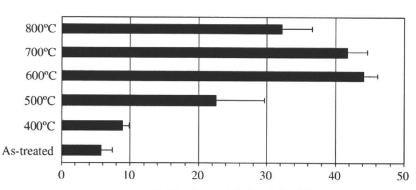

Fig. 3 Scratch resistances of surfaces of Ti metals subjected to heat treatments at various temperatures after NaOH and HCl treatments

temperatures after NaOH and HCl treatments. From Fig. 3, it can be seen that the scratch resistance of the surface of the Ti metal was as low as 5 mN after the NaOH and HCl treatments, and this increased to 45 mN with increasing heat treatment temperature up to 600°C, and that the scratch resistance decreased for heat treatment temperatures above 700°C.

3.2 Apatite-forming ability of treated Ti metal in an SBF

Figure 4 shows FE-SEM photographs of the surface of Ti metal soaked in an SBF for 1 day after heat treatment at various temperatures following NaOH and HCl treatments. A small number of spherical particles was observed on the surface of the Ti metal treated with NaOH and HCl solutions, and the number of these particles increased with increasing heat treatment temperature up to 700°C, and then decreased for a heat treatment temperature of 800°C.

Figure 5 shows the TF-XRD patterns of Ti metal soaked in an SBF for 1 day after heat treatment at various temperatures following NaOH and HCl treatments. From Fig. 5, it can be seen that apatite had precipitated on the Ti metal heat-treated at temperatures in the range 500–700°C. These results indicate that the spherical particles observed on the surface of the Ti metal samples in Fig. 4 were composed of apatite.

3.3 Zeta potential of treated Ti metal

Figure 6 shows the zeta potential of the surface of Ti metal subjected to heat treatment at various temperatures

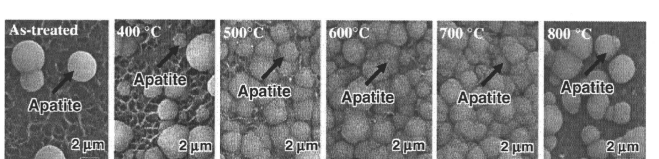

Fig. 4 FE-SEM photographs of surfaces of Ti metals soaked in SBF for 1 day, after heat treatments at various temperatures following the NaOH and HCl treatments

Author's personal copy

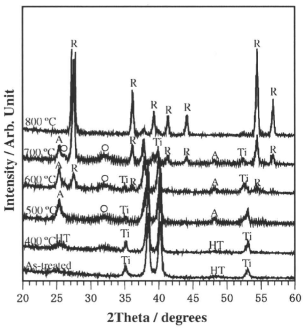

Fig. 5 TF-XRD patterns of the surfaces of Ti metals soaked in SBF for 1 day after heat treatments at various temperatures following the NaOH and HCl treatments. *Ti* α Titanium, *HT* Hydrogen titanate, *A* anatase, *R* Rutile, *O* Apatite

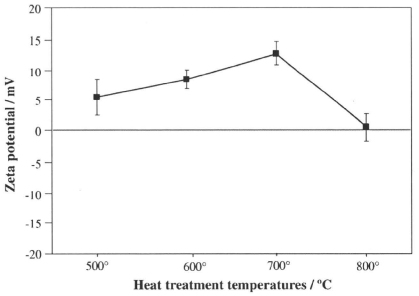

Fig. 6 Zeta potentials of surfaces of Ti metals subjected to heat treatments at various temperatures after NaOH and HCl treatments

following NaOH and HCl treatments. The zeta potential of the samples that had been heat-treated at temperatures below 400°C was not able to be measured, because no, or only a thin, insulating titanium oxide layer had formed on the surface. The Ti metal heat-treated at temperatures in the range 500–700°C exhibited a positive zeta potential that increased with increasing heat treatment temperature up to 700°C, while the Ti metal samples heat-treated at 800°C exhibited a zeta potential of zero.

3.4 XPS spectra of treated Ti metal

Figure 7 shows the XPS spectra of the Ca and P ions on the surface of the Ti metal samples subjected to heat treatment at 400, 600, and 800°C as a function of the soaking time in an SBF after NaOH and HCl treatments. From Fig. 7, it can be seen that Ti metal treated with NaOH and HCl solutions that was subsequently heat-treated at 400°C adsorbed both calcium and phosphate ions almost simultaneously on its surface from the initial stages of soaking in the SBF, whereas Ti metal samples heat-treated at 600 and 800°C only adsorbed phosphate ions during the early stages of soaking in the SBF.

Figure 8 shows the XPS spectra of Cl ions of the surface of Ti metal subjected to heat treatment at 600 and 800°C after NaOH and HCl treatments. From Fig. 8, it can be seen that Cl ions were adsorbed on the surface of the Ti metal after the NaOH and HCl treatments, and that these ions remained on the surface even after the subsequent heat treatment at 600°C, but the samples showed a slight decrease in the number of Cl ions after a heat treatment at 800°C.

4 Discussion

It is apparent from the experimental results described above that the nanometer scale roughness formed on the surface of Ti metal after the NaOH treatment remained after the HCl treatment, and even after a subsequent heat treatment at temperatures below 700°C (see Fig. 1). The decrease in roughness at a heat treatment temperature of 800°C is because of sintering and thickening of the surface oxide layer. The NaOH- and HCl-treated Ti metal formed titanium oxide of anatase and rutile phases when heat-treated at temperatures above 500°C (see Fig. 2).

The scratch resistance of the surface of NaOH- and HCl-treated Ti metal increased with the formation of a titanium oxide layer for heat treatment temperatures above 500°C, but decreased for a heat treatment temperature of 800°C. This decrease may be attributed to the difference in thermal expansion coefficients between the Ti metal substrate and the thick titanium oxide layer.

The titanium oxide formed on the NaOH- and HCl-treated Ti metal samples showed a high apatite-forming ability in an SBF when the temperature of the heat treatment was in the range 500–700°C. This high apatite-forming ability was not attributable to the surface roughness, since the surface roughness of Ti metal samples heat-treated in this temperature range was not different from that of samples heat-treated at lower temperature. Nor was it attributable to a specific crystalline phase, as the ratio of rutile to anatase on the surface of the Ti metal samples was largely changed in this temperature range (see Fig. 2). Therefore, the high apatite-forming ability was attributed to the positive surface charge, as the Ti metal samples only showed a positive zeta potential when the samples were heat-treated in the temperature range of 500–700°C (see Fig. 6). When the Ti metal samples had a positively charged surface,

Author's personal copy

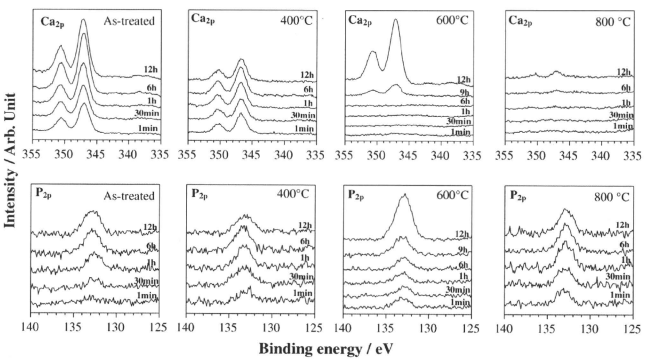

Fig. 7 XPS spectra of Ca and P of the surface of Ti metals as a function of soaking period in SBF subjected to heat treatments at 400, 600 and 800°C after NaOH and HCl treatments

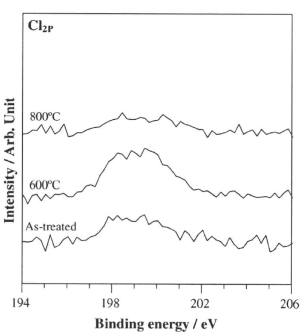

Fig. 8 XPS spectra of Cl ion on the surface of Ti metals as a function of soaking period in SBF subjected to heat treatments at 600 and 800°C after NaOH and HCl treatments

negatively charged phosphate ions were selectively adsorbed on the surface in the SBF. As the phosphate ions begin to accumulate, the surface becomes negatively charged, and, therefore, positively charged calcium ions are adsorbed on the surface to form an apatite layer. This sequential adsorption of phosphate and calcium ions on the Ti metal samples was confirmed by the XPS spectra of Ti metal samples heat-treated at 600°C after NaOH and HCl treatments (see Fig. 7). According to the data in Fig. 7, Ti metal samples heat-treated at 800°C also showed an initial selective adsorption of phosphate ions. However, this tendency was weak. Both Ti metal samples treated with NaOH and HCl solutions and those subsequently heat-treated at 400°C did not show any selective adsorption of phosphate ions, but showed the simultaneous adsorption of calcium and phosphate ions (see Fig. 7). When the calcium and phosphate ions were adsorbed simultaneously on the surface, then its charge was soon neutralized and the calcium phosphate formed could not grow to form an apatite layer.

The reason for the positive surface charge of Ti metal samples heat-treated in the temperature range 500–700°C was attributed to the presence of chloride ions that were adsorbed on the hydrogen titanate layer formed on the Ti metal after the HCl treatment. These remained on the surface, even after the conversion of the hydrogen titanate into titanium oxide by a heat treatment below 700°C. The adsorbed chloride ions dissociate from the surface of the titanium oxide in an SBF to create an acidic environment on the Ti metal. Titanium oxide has been reported to have a positively charged surface in an acidic environment [1]. Above a temperature of 800°C, the chloride ions on the surface of the titanium oxide decompose (see Fig. 8), and so do not form a strong acidic environment and a positive surface charge in an SBF.

Recently, it was reported that Ti metal subjected to a mixed acid treatment shows high apatite-forming ability when it was heat-treated at temperatures ranged from 500 to 650°C, and that their high apatite-forming abilities are also attributed to their positive surface charge [15]. This is consistent with the present results.

It has been reported that osteoconduction and osteoinduction are closely related to an apatite-forming ability [16]. Our present results could establish the fundamental conditions required for chemical and heat treatments to obtain porous titanium metal that could induce high osteoconductivity and osteoinductivity.

5 Conclusions

1. A nanometer scale roughness formed on Ti metal samples after an NaOH treatment remains after an HCl

Author's personal copy

treatment and a subsequent heat treatment below 700°C.

2. NaOH- and HCl-treated Ti metal forms titanium oxide of anatase and rutile phases on its surface after a heat treatment above 500°C.
3. The scratch resistance of the surface of Ti metal increases with the formation of titanium oxide up to 700°C, and then decreases with increasing temperature.
4. The apatite-forming ability in an SBF of Ti metal is remarkably high when the Ti metal is heat-treated in the temperature range 500–700°C after NaOH and HCl treatments.
5. The high apatite-forming ability of Ti metal subjected to the above treatments is attributed to positive surface charges.
6. These positive surface charges arise from the presence of chloride ions adsorbed on the titanium oxide layer, which dissociate in an SBF to give an acidic environment.
7. Our present results could establish the conditions required for the chemical and heat treatments to obtain porous Ti metal oxide that could induce high osteoconductivity and osteoinductivity.

References

1. Textor M, Sittig C, Frauchiger V, Tosatti S, Brunette DM. Properties and biological significance of natural oxide films on titanium and its alloys. In: Brunette DM, Tengvall P, Textor M, Thomsen P, editors. Titanium in medicine. Germany: Springer; 2001. p. 171–230.
2. Hacking SA, Tanzer M, Harvey EJ, Krygier JJ, Bobyn JD. Relative contributions of chemistry and topography to the osseointegration of hydroxyapatite coatings. Clin Orthop Relat Res. 2002;405:24–38.
3. Kokubo T, Miyaji F, Kim HM, Nakamura T. Spontaneous formation of bonelike apatite layer on chemically treated titanium metals. J Am Ceram Soc. 1996;79:1127–9.
4. Kim HM, Miyaji F, Kokubo T, Nakamura T. Preparation of bioactive Ti and its alloy via simple chemical surface treatment. J Biomed Mater Res. 1996;32:409–17.
5. Yan WQ, Nakamura T, Kobayashi M, Kim HM, Miyaji F, Kokubo T. Bonding of chemically treated titanium implants to bone. J Biomed Mater Res. 1997;37:267–75.
6. Nishiguchi S, Fujibayashi S, Kim HM, Kokubo T, Nakamura T. Biology of alkali- and heat-treated titanium implants. J Biomed Mater Res. 2003;67A:26–35.
7. Kawanabe K, Ise K, Goto K, Akiyama H, Nakamura T, Kaneuji A, Sugimori T, Matsumoto T. A new cementless total hip arthoplasty with bioactive titanium porous-coating by alkaline and heat treatment: average 4.8-year results. J Biomed Mater Res. 2009;90B:476–81.
8. Pattanayak DK, Kawai T, Matsushita T, Takadama H, Kokubo T, Nakamura T. Effect of HCl concentrations on apatite-forming ability of NaOH-HCl- and heat-treated titanium metal. J Mater Sci Mater Med. 2009;20:2401–11.
9. Takemoto M, Fujibayashi S, Neo M, Suzuki J, Kokubo T, Nakamura T. Mechanical properties and osteoconductivity of porous bioactive titanium. Biomaterials. 2005;26:6014–23.
10. Takemoto M, Fujibayashi S, Neo M, Suzuki J, Matsushita T, Kokubo T, Nakamura T. Osteoinductive porous titanium implants: effect of sodium removal by dilute HCl treatment. Biomaterials. 2006;27:2682–91.
11. Takemoto M, Fujibayashi S, Neo M, So K, Akiyama N, Matsushita T, Kokubo T, Nakamura T. A porous bioactive titanium implant for spinal interbody fusion: an experimental study using a canine model. J Neurosurg Spine. 2007;7:435–43.
12. Kokubo T, Takadama H. How useful is SBF in predicting in vivo bone bioactivity? Biomaterials. 2006;27:2907–15.
13. Sun X, Li Y. Synthesis and characterization of ion-exchangeable titanate nanotubes. Chem Eur J. 2003;9:2229–38.
14. Tsai CC, Teng H. Structural features of nanotubes synthesized from NaOH treatment on TiO_2 with different post-treatments. Chem Mater. 2006;18:367–73.
15. Kokubo T, Pattanayak DK, Yamaguchi S, Takadama H, Matsushita T, Kawai T, Takemoto M, Fujibayashi S, Nakamura T. Positively charged bioactive titanium metal prepared by simple chemical and heat treatments. J R Soc Interface. 2010;7:S503–13.
16. Bruijn JDD, Shankar K, Yuan H, Habibovic P. Osteoinduction and its evaluation. In: Kokubo T, editor. Bioceramics and their clinical applications. Cambridge: Woodhead publishing Ltd; 2008. p. 199–219.